Acta Crystallographica Section D
Biological Crystallography
ISSN 0907-4449

Structure of a red fluorescent protein from *Zoanthus*, zRFP574, reveals a novel chromophore

Nadezhda Pletneva,[a] Sergei Pletnev,[b,c] Tamara Tikhonova,[d] Vladimir Popov,[d] Vladimir Martynov[a] and Vladimir Pletnev[a]*

[a]Shemyakin–Ovchinnikov Institute of Bioorganic Chemistry, Russian Academy of Science, Moscow, Russia, [b]Institute of Crystallography, Russian Academy of Science, Moscow, Russia, [c]Synchrotron Radiation Research Section, MCL, National Cancer Institute, Argonne National Laboratory, Argonne, IL 60439, USA, and [d]Bakh Institute of Biochemistry, Russian Academy of Science, Moscow, Russia

Correspondence e-mail: pletnev@hwi.buffalo.edu

Received 23 January 2006
Accepted 3 March 2006

PDB Reference: zRFP574, 2fl1, r2fl1sf.

The three-dimensional structure of the red fluorescent protein (RFP) zRFP574 from the button polyp *Zoanthus* sp. (two dimers per asymmetric unit, 231 × 4 amino acids) has been determined at 2.4 Å resolution in space group $C222_1$. The crystal structure, refined to a crystallographic R factor of 0.203 ($R_{\rm free}$ = 0.249), adopts the β-barrel fold composed of 11 strands similar to that of the yellow fluorescent protein zYFP538. The zRFP574 chromophore, originating from the protein sequence Asp66-Tyr67-Gly68, has a two-ring structure typical of GFP-like proteins. The bond geometry of residue 66 shows the strong tendency of the corresponding C^{α} atom to sp^2 hybridization as a consequence of *N*-acylimine bond formation. The zRFP574 chromophore contains the 65–66 *cis*-peptide bond characteristic of red fluorescent proteins. The chromophore phenolic ring adopts a *cis* conformation coplanar with the imidazolinone ring. The crystallographic study has revealed an unexpected chemical feature of the internal chromophore. A decarboxylated side chain of the chromophore-forming residue Asp66 has been observed in the structure. This additional post-translational modification is likely to play a key role in the bathochromic shift of the zRFP574 spectrum.

1. Introduction

The green fluorescent protein (GFP) and GFP-like proteins from marine organisms exhibit an extraordinary ability to spontaneously generate fluorescence in living cells. This property has found broad application in biochemistry, cell biology and biotechnology for monitoring of gene expression, protein localization and other vital cellular functions (Chalfie & Kain, 1998; Tsien, 1998; Verkhusha & Lukyanov, 2004; Zubova *et al.*, 2003). The GFP family comprises homologous 25–30 kDa proteins that cover the emission range 442–645 nm with an emission spectrum from blue to red. The large spectral diversity of the fluorescent proteins mostly arises from variations in the chemical structure of the mature chromophore. The red-shifted fluorescent proteins (RFPs) are in high demand for various applications, providing additional tools for multicolour labelling. Compared with GFP, the RFPs have longer wavelength emission, which helps to overcome the interfering cell autofluorescence and results in higher sensitivity (Gurskaya *et al.*, 2001). The chromophore of the FPs forms autocatalytically from residues 66–68 (according to zYFP538 numbering; Remington *et al.*, 2005) without the need for any cofactors, enzymes or chaperones except for molecular oxygen. The nature of residue 66 (*X*66) does not seem to play a key role in the chromophore synthesis; however, it is important for the yellow fluorescence of zYFP538 (Remington *et al.*, 2005) and the red fluorescence of the Kaede-like

Table 1
Crystallographic data and refinement statistics.

Values in parentheses are given for the last resolution shell (2.5–2.4 Å).

Space group	$C222_1$
Unit-cell parameters (Å)	a = 114.9, b = 146.8, c = 122.9
Monomers per cell (Z)	32
Estimated solvent content (%)	50
Temperature (K)	100
Wavelength (Å)	1.54
Resolution range (Å)	30–2.4
Total reflections measured	213225
Unique reflections observed	40878
$I/\sigma(I)$	7.8 (1.5)
$R_{\rm merge}$	0.135 (0.664)
Completeness	99.9 (99.9)
Non-H atoms in model	
Protein (4 × 231 residues)	7296
SO_4^{2-} (9 × 5)	45
Water ($\rho \geq 3\sigma$)	412
$R_{\rm work}$ (95% data, $F \geq 0$)	0.203
$R_{\rm free}$ (5% data, $F \geq 0$)	0.249
Average B factor (Å^2)	
Protein	28.6
Chromophore	22.4
SO_4^{2-}	38.9
Water	31.3
R.m.s. deviations	
Bond distance (Å)	0.008
Bond angle (°)	1.54
Planarity (°)	1.73
Dihedral angle (°)	25.9
Coordinate error (5.0–2.4 Å shell)	
$\sigma_{\rm A}$	0.27
$\sigma_{\rm A}$ (cross-validated)	0.34
Ramachandran plot statistics (for 791 non-Gly/Pro residues) (%)	
Most favoured and additional allowed regions	100

proteins (Ando *et al.*, 2002; Pakhomov *et al.*, 2004; Wiedenmann *et al.*, 2004). The positions 67 and 68 are invariant in all known wild-type FPs and are occupied by Tyr and Gly, respectively. In most cases, post-translational modification results in an imidazolinone heterocycle with a *p*-hydroxybenzylidene substituent. According to the proposed general mechanism, the peptide cyclization is initiated by nucleophilic attack of the Gly68 amide N atom on the *X*66 carbonyl C atom to create a five-membered imidazolinone ring, followed by dehydration and rate-limiting oxidation of the Tyr67 $C^{\alpha}-C^{\beta}$ bond to conjugate the ring systems. To date, the structural and chemical features that cause the chromophore formation and the mechanism of its fluorescence are not fully understood.

The red-emitting fluorescent protein zRFP574 from the button polyp *Zoanthus* sp. (MW 26.4 kDa; 231 amino-acid residues) is characterized by the chromophore-forming sequence Asp66-Tyr67-Gly68 and light excitation at 553 nm and emission at 574 nm (Labas *et al.*, 2002; Yanushevich *et al.*, 2003). zRFP574 is very similar to the red fluorescent protein DsRed (*Discosoma* sp.; Matz *et al.*, 1999) in the shape of its excitation/emission curves and matures similarly to the DsRed timer mutant (Terskikh *et al.*, 2000). At the beginning of the maturation process it emits green light and at the final stages turns red (Yanushevich *et al.*, 2003). zRFP574 shares ∼75% sequence identity with the yellow fluorescent protein zYFP538, which is characterized by the chromophore-forming sequence Lys66-Tyr67-Gly68 and emission at 538 nm. The crystal structure of zYFP538 revealed a novel chromophore with a third six-membered ring possibly resulting from a transamination reaction of the Lys66 side chain with *N*-acylimine (Remington *et al.*, 2005).

In this paper, we present new structural details revealed by an X-ray study of its close homologue zRFP574.

2. Materials and methods

2.1. Purification and crystallization

The plasmid pQE30-zRFP574 was a generous gift from K. A. Lukyanov (Shemyakin–Ovchinnikov Institute of Bioorganic Chemistry, RAS, Moscow). The plasmid pQE30-zRFP574 was transformed into cells of *Escherichia coli* strain JM109 DE3. The protein with an N-terminal His-tag fragment was expressed on LB-Amp Petri plates by overnight incubation at 310 K followed by two days storage at 293 K for complete protein maturation. Cells were resuspended in 20 m*M* Tris–HCl pH 8.0, 100 m*M* NaCl (buffer *A*) and disrupted by sonification. The cell extract was clarified by centrifugation. Purification was carried out using a metal-affinity column (Ni–NTA, Qiagen). Protein solution was applied onto the column and extensively washed with buffer *A*. Elution of the protein was accomplished with 100 m*M* EDTA in buffer *A*. Final purification was achieved by size-exclusion chromatography on a Superdex 75 HiLoad (16/60) column (Pharmacia) in 20 m*M* Tris–HCl pH 7.5, 200 m*M* NaCl elution buffer at 277 K. The sample was eluted from the column as two peaks at volumes of 43 and 51 ml. SDS–PAGE showed that the first peak contained three distinct high-molecular-weight aggregates, whereas the second peak consisted mainly of one homogeneous specimen. Peaks were collected separately and concentrated in VivaSpin 10 kDa molecular-weight cutoff concentration units (VivaScience).

The homogeneous sample from the second peak was used for crystallization. Cube-shaped crystals were grown at 293 K from 1.4–1.6 *M* $(NH_4)_2SO_4$, 0.2 *M* potassium/sodium tartrate and 0.1 *M* sodium citrate buffer pH 5.9. Crystals appeared within a few days, achieving final dimensions of 0.15 × 0.15 × 0.15 mm in about eight weeks.

N-terminal amino-acid miCRR sequencing of the protein sample was performed by the Edman degradation method on an ABI 494 Protein Sequencer.

2.2. Structure solution and crystallographic refinement

Low-temperature X-ray diffraction data were collected on a MAR 345 image-plate detector coupled with a RU-200 X-ray generator and were processed with the *HKL*2000 program suite (Otwinowski & Minor, 1997). Crystallographic data are presented in Table 1. The calculated Matthews coefficient of 2.45 Å^3 Da^{-1} indicated the probable presence of four protein subunits in the asymmetric unit. The crystal structure was determined by the molecular-replacement technique with the *MOLREP* program from the *CCP*4 crystallographic package (Collaborative Computational Project, Number 4, 1994). The

use of the coordinates of the monomer mutant Lys66Met of the yellow fluorescent protein zYFP538 (*Zoanthus* sp.; 75% sequence identity; PDB code 1xa9; Remington *et al.*, 2005) as a search probe resulted in four solutions confirming the Matthews coefficient estimation.

Crystallographic refinement was performed with the *CNS* software package (Brünger *et al.*, 1998) using consecutively strict and restrained non-crystallographic symmetry. In the final stage of refinement, four subunits in the asymmetric unit were refined independently. All steps of the refinement process included manual adjustment of the model in the electron density using the graphics program *CHAIN* (Sack, 1988). A summary of the crystallographic data and refinement statistics is presented in Table 1.

Analysis of the molecular geometry was performed with *CNS*, *CCP*4 and *PROCHECK* (Laskowski *et al.*, 1993). The illustrations were produced with the *SETOR* (Evans, 1993), *LIGPLOT*/*HBPLUS* (Wallace *et al.*, 1995; McDonald & Thornton, 1994) and *ACD ChemSketch* v.5/12 (http://www.acdlabs.com) programs.

3. Results and discussion

3.1. Electron-density interpretation

The observed electron density is generally in good agreement with the known protein sequence. It allowed unambiguous fitting of residues 4–231 of the known protein sequence for all four (*A*, *B*, *C*, *D*) monomers in the asymmetric unit. The $2F_o - F_c$ simulated-annealing omit map and $F_o - F_c$ difference map unequivocally confirmed the two-ring structure of the chromophore and revealed the absence of the carboxyl group at the expected Asp66 side chain. No density was found for the N-terminal His-tag fragment introduced into the native construct and used for protein purification. The results of the N-terminal sequencing indicated Ser4 as the first residue of the protein sequence, in accordance with the observed electron density. The most probable explanation of this observation could be protease contamination in solution after protein isolation and purification. However, the β-barrel fold of zRFP574 was found to be intact, probably owing to the high resistance of GFP-like proteins to proteolysis (Bokman & Ward, 1981; Martynov *et al.*, 2003).

Several side chains of the structure are likely have second stable alternative orientations, which could be identified with confidence at higher resolution. Subunit *D*, in sharp contrast to other subunits, shows weak discontinuous density for a number of side chains of Glu, Lys and Arg residues and of those in the loop regions 114–117 and 192–194. The specifically shaped electron density in nine local regions was assigned to partially occupied SO_4^{2-} ions (a component of the crystallization solution) linked to the nearest Arg and Lys side chains by salt bridges. A total of 412 well ordered water molecules corresponding to an electron-density level $\rho \geq 3\sigma$ form the hydrogen-bonded hydration shell for all four subunits. Other weaker density, most likely to correspond to partially disordered and partially occupied solvent, lacks confident interpretation at the current resolution.

3.2. Overall structure and monomer association

There are two dimers, *AD* and *BC*, in the asymmetric unit. In each dimer, the cylindrically shaped monomers (β-barrel shape; Tsien, 1998) are related by a non-crystallographic twofold pseudosymmetry axis perpendicular to antiparallel β-barrel axes. The dimers are oriented at $\sim$65° to each other, with a rather weak interface between their termini. The tightly packed tetrameric assemblies, *ADA′D′* and *BCB′C′*, similar to those of zYFP538, are generated from corresponding dimers with side packing at $\sim$90° as a result of the crystallographic symmetry operations $-x-1, y, -z-1/2$ and $-x, y, -z-1/2$, respectively (Fig. 1). The dimers are related by a crystallographic twofold symmetry axis running through the tetrameric assembly at $\sim$45° towards the β-barrel axes.

The tetrameric assemblies are characterized by two types of interfaces between intermonomer contacting surfaces, *AD* (or *BC*) and *AA′* (or *BB′*). The interface *AD* (*BC*) is built by a

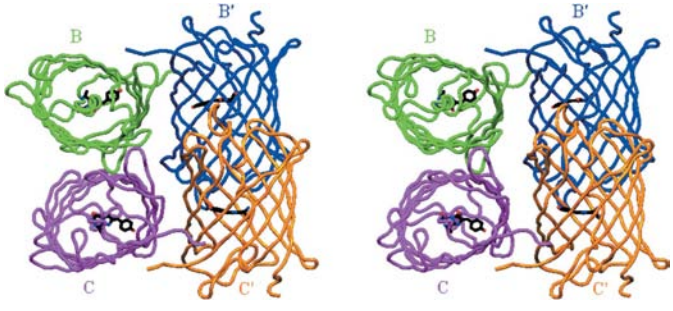

Figure 1
Stereoview of zRFP574 tightly packed tetramer assembly *BCB′C′*, where *B′* and *C′* are symmetry-related subunits. Figure produced using *SETOR* (Evans, 1993).

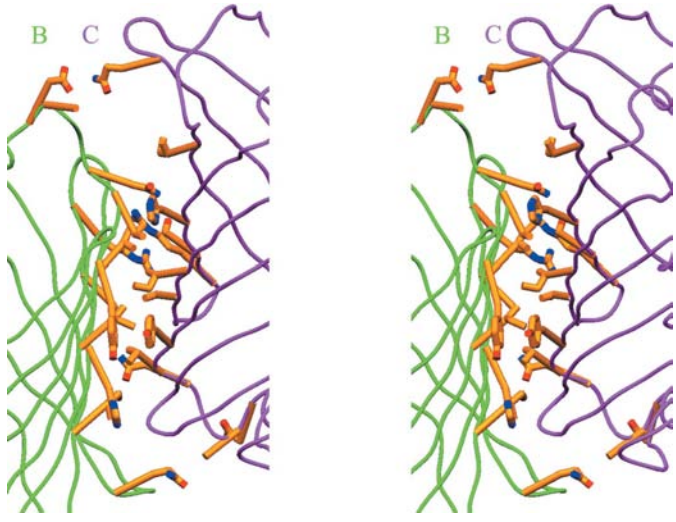

Figure 2
Stereoview of the interface between *B* and *C* subunits related by twofold non-crystallographic symmetry. Figure produced using *SETOR* (Evans, 1993).

double set of side chains of His94, Ser96, Arg98, Val104, Ile106, Tyr127, Val129, Asp130, Ala133, Asp134, Gln158 and Ile184 residues from antiparallel monomers (Fig. 2). This association is mostly stabilized by hydrophobic interactions in the central hydrophobic cluster. The more extensive and energy-stable interface AA' (BB') is composed from a strictly symmetry-related double set of side chains from Gln146, Pro147, Cys149, Lys151, Ile153, Lys162, Asp164, Ser166, Tyr168, Arg176, Arg178, Gln180, Trp197, Phe199, Gln201, Lys203, His222, Ile224, Ala229, Leu230 and Pro231 residues (Fig. 3). Apart from a number of hydrophobic contacts, the double set of four hydrogen bonds [Asp164···Tyr168, Asp164···Ser166, Gln201···Ala229 (N—H), Lys203···Leu230 (C═O)] and three salt bridges [Glu146···Lys151, Asp164···Arg178, Lys203···Pro231 (terminal C═O)] make (mostly between the side chains) a significant stabilizing contribution. The symmetry-related Cys149 residues from both monomers in the contact area are spatially close, bringing the S atoms to a distance of 3 Å in the alternative optimal side-chain orientations. It is the most probable source of possible disulfide bridging in the aggregation process detected during the protein purification stage. The tightly packed tetramer has an accessible surface area of 33 966 Å^2 for a probe radius of 1.4 Å and the area buried at interfaces owing to tetramerization is 7581 Å^2 or ∼18% of the total surface of the four monomers (41 547 Å^2). The observed structure at the interfaces provides a basis for the rational choice of site-directed mutagenesis experiments to design stable monomeric forms of fluorescent markers for practical applications.

The β-barrel fold of the zRFP574 monomer is similar to that of the homologous zYFP538, with a root-mean-square deviation (r.m.s.d.) of 0.65 Å for all 227 equivalent C$^\alpha$ atoms (Fig. 4). Two *cis*-peptide bonds preceding Pro53 and Pro88

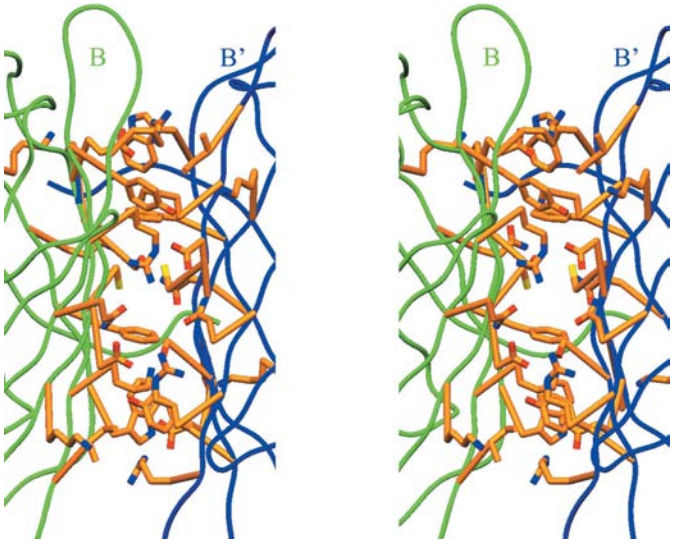

Figure 3
Stereoview of the interface between B and B' subunits related by twofold crystallographic symmetry. Figure produced using *SETOR* (Evans, 1993).

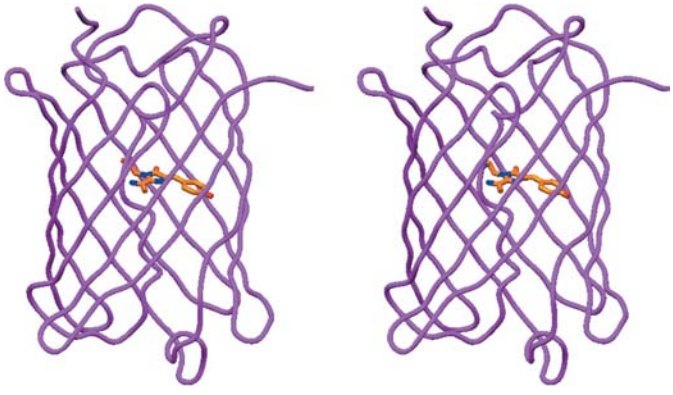

Figure 4
Stereoview of the zRFP574 β-barrel fold with the chromophore in the centre. Figure produced using *SETOR* (Evans, 1993).

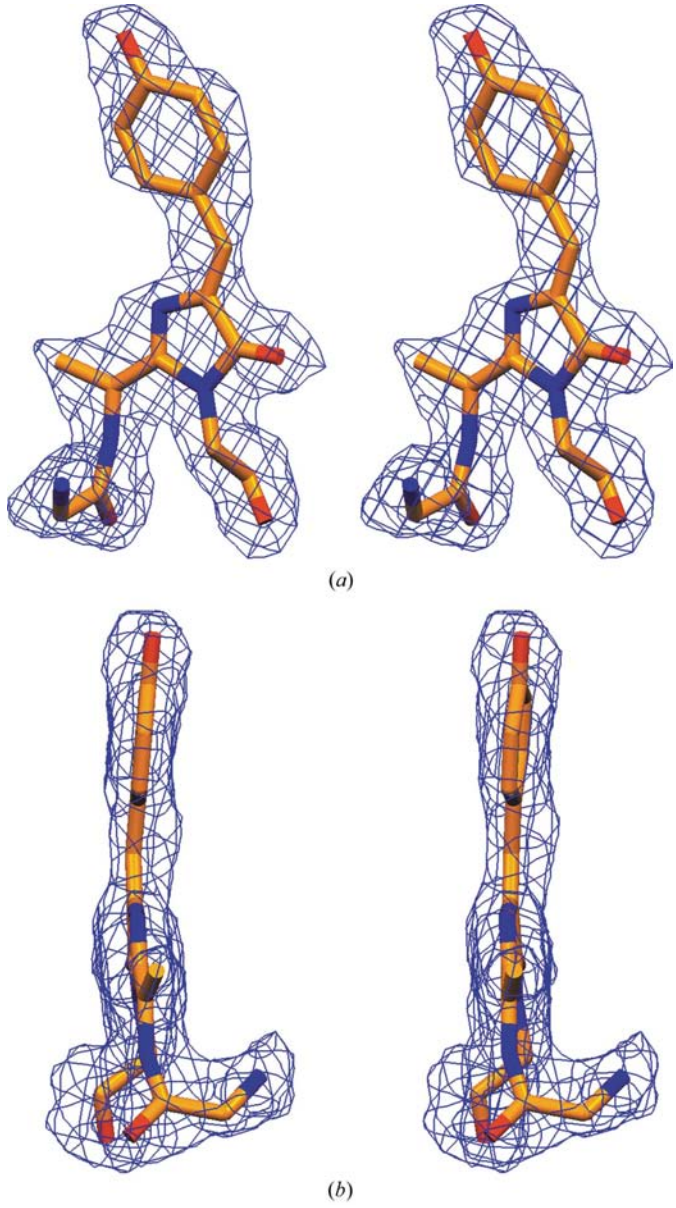

Figure 5
Side (*a*) and edge (*b*) stereoviews of the zRFP574 chromophore with the backbone of the preceding residue in $2F_o - F_c$ electron density (cutoff $\rho \geq 1.3\sigma$). Figure produced using *SETOR* (Evans, 1993).

have been detected in the structure. It has a bicyclic chromophore located on a distorted α-helix (58–71) near the geometric centre of the 11-stranded β-barrel. The loop fragments between β-strands (22–24, 50–57, 99–102, 130–142, 171–175, 211–214 and 6–10, 37–40, 75–89, 115–118, 156–159, 188–197) form two flanking caps at the ends of the β-barrel, protecting access to its internal area. Only 7–10 of the 412 ordered water molecules have been found inside β-barrels along the distorted α-helix. Of these, five are located in close vicinity of the chromophore.

3.3. Chromophore structure

According to a recently proposed hypothesis, steric interactions generated by the GFP-like protein architecture raise the precyclization-state energy, causing a dramatic bend in the central α-helix and driving chromophore formation (Barondeau *et al.*, 2003). In addition to the steric factor, several residues in close proximity to the chromophore provide a scaffold for specific functional group chemistry to accelerate chromophore maturation.

The crystallographic study of zRFP574 has revealed an unexpected chemical structure of the internal chromophore originating from the protein sequence Asp66-Tyr67-Gly68. The chromophore maturation results in a typical GFP two-ring structure characterized by a decarboxylated side chain of the expected Asp66 (*X*66) residue (Figs. 5 and 6). Like the DsRed crystal structure (Yarbrough *et al.*, 2001), the zRFP574 chromophore contains an unusual *cis*-peptide bond preceding *X*66. The phenolic ring of Tyr67 moves into the chromophore plane in *cis* orientation to the Tyr67 $C^{\alpha}-N$ bond. The torsion angles of 5.6 and -7.3° around the corresponding $C^{\alpha}-C^{\beta}$ and $C^{\beta}-C^{\gamma}$ bonds of Tyr67 define its close coplanar arrangement with the chromophore five-membered imidazolinone ring. It was proposed (Chudakov *et al.*, 2003) and experimentally confirmed (Andresen *et al.*, 2005) that the *cis* orientation of the *p*-hydroxybenzylidene ring in GFP-like proteins accompanies their active fluorescent state. In the zRFP574 structure, it makes effective stacking interactions (at 3.4 Å distance) with the parallel imidazole ring of the proximal His202 residue. The formation of the *N*-acylimine partial double bond, $N{=}C^{\alpha}$, in residue *X*66 results in considerable flattening of the bond geometry around the C^{α} atom, evidence of its strong tendency to sp^2 hybridization. This most likely extends the system conjugation, resulting in a bathochromic shift of the protein spectrum.

The stereochemical environment of the chromophore (Fig. 7) presumably includes catalytic residues participating in chromophore formation. Among them are the non-conserved Ala63 (with position equivalent to Thr62 in GFP) and the conserved Arg95 and Glu221 residues. According to the proposed mechanism (Barondeau *et al.*, 2003; Wood *et al.*, 2005), the positively charged side chain of Arg95 acidifies the Gly68 backbone N and/or Tyr67 C^{α} atoms, promoting their deprotonation. The carbonyl O atom of Ala63 and the O atom of the Glu221 side chain may serve as the bases, abstracting the protons to favour either or both of these deprotonation reactions. The Gly68 N-atom deprotonation would facilitate main-chain cyclization through a nucleophilic attack of the nitrogen lone pair on the Asp66 carbonyl C atom.

The severe electrostatic conflict between the spatially close negatively charged side chains of the chromophore Asp66 and the proximal Glu221 is likely to be the trigger initiating the observed Asp66 decarboxylation. The nature of the long-range electrostatic interactions may facilitate the process. Currently, the mechanism of this process remains unclear. The side chains of the Gln42 and Arg70 residues and the adjacent water molecule, all of which are hydrogen bonded to Glu221, may possibly participate in this reaction as proton donors. We also cannot exclude the mechanism proposed for the light-dependent decarboxylation of avGFP. This mechanism

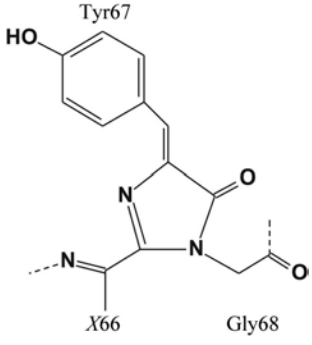

Figure 6
Chemical structure of zRFP574 chromophore. This figure was produced using *ChemSketch* (http://www.acdlabs.com).

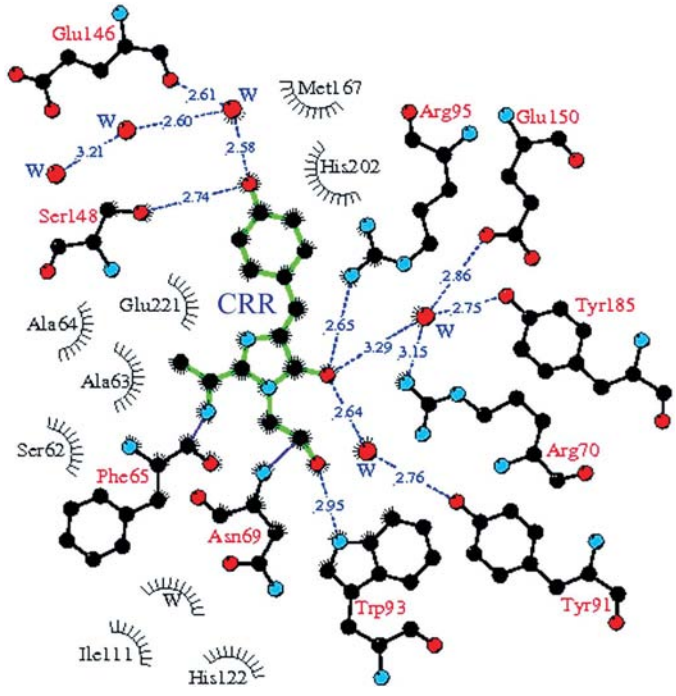

Figure 7
Schematic illustration of the chromophore (CRR) environment. Hydrogen bonds (≤3.3Å) are shown by blue dashed lines, waters (W) by red spheres and van der Waals contacts (≤3.9Å) by black 'eyelashes'. This figure was produced using *LIGPLOT*/*HBPLUS* (Wallace *et al.*, 1995; McDonald & Thornton, 1994).

presumes chromophore moiety participation in proton and alternate electron transfer upon oxidative decarboxylation of the neighbouring Glu221 residue (van Thor *et al.*, 2002).

The protein side chains of Trp93, Arg95 and Ser148 make direct hydrogen bonds with the Gly68 C═O, Tyr67 C═O and Tyr67 OH chromophore groups, respectively. It has been proposed that the positively charged guanidinium group of Arg95 electrostatically stabilizes increased electron density on the corresponding carbonyl O atom in the chromophore's excited state (Tsien, 1998). The distance range of 3.2–3.6 Å between the Glu221 carboxyl O atom and the chromophore Tyr67 N most likely indicates a deprotonated state of the N atom and a possible mediating role of the corresponding hydrogen bond with the protonated atom in the maturation process. Five water molecules (W) mediate hydrogen bonding between the chromophore and the nearest amino-acid functional groups. W1 bridges Tyr67 OH and Glu146 C═O. W2 and W3 connect Tyr67 C═O with Tyr91 OH and with Arg70 NH_2, Glu150 $O^{\varepsilon1}$, Tyr185 OH, respectively, and W4 connects Phe65 C═O with Asn69 $N^{\delta2}$. W5 is located at hydrogen-bonding distances from Arg70 NH_2, Glu221 $O^{\varepsilon1}$, Asn69 C═O and Asn69 N. Water molecules W3, W4 and W5 might be the probable products of the reactions resulting in the Tyr67 C^{α}═C^{β}, *X*66 C^{α}═N and *X*66 Gly68 C═N bonds, respectively, in the mature chromophore.

We thank Dr K. A. Lukyanov for providing us with the plasmid pQE30-zRFP574. This work was supported by EOARD under ISTC Partner Project No. 3223, Russian Foundation for Basic Research (grant No. 06-04-48196) and a grant from the Russian Academy of Sciences for the program Molecular and Cellular Biology (No. 200101) and in part by the Intramural Research Program of the NIH, National Cancer Institute, Center for Cancer Research. The content of this publication does not necessarily reflect the views or policies of the Department of Health and Human Services, nor does mention of trade names, commercial products or organizations imply endorsement by the US or any other Government.

References

Ando, R., Hama, H., Yamamoto-Hino, M., Mizuno, H. & Miyawaki, A. (2002). *Proc. Natl Acad. Sci. USA*, **99**, 12651–12656.

Andresen, M., Wahl, M. C., Stiel, A. C., Grater, F., Schafer, L. V., Trowitzsch, S., Weber, G., Eggeling, C., Grubmuller, H., Hell, S. W. & Jakobs, S. (2005). *Proc. Natl Acad. Sci. USA*, **102**, 13070–13074.

Barondeau, D. P., Putnam, D. C., Kassmann, C. J., Tainer, J. A. & Getzoff, E. D. (2003). *Proc. Natl. Acad. Sci. USA*, **100**, 12111–12116.

Bokman, S. H. & Ward, W. W. (1981). *Biochem. Biophys. Res. Commun.* **101**, 1372–1380.

Brünger, A. T., Adams, P. D., Clore, G. M., DeLano, W. L., Gros, P., Grosse-Kunstleve, R. W., Jiang, J.-S., Kuszewski, J., Nilges, M., Pannu, N. S., Read, R. J., Rice, L. M., Simonson, T. & Warren, G. L. (1998). *Acta Cryst.* D**54**, 905–921.

Chalfie, M. & Kain, S. (1998). *GFP Green Fluorescent Protein. Properties, Applications and Protocols.* New York: Wiley-Liss.

Chudakov, D. M., Feofanov, A. V., Mudriku, N. N., Lukyanov, S. & Lukyanov, K. A. (2003). *J. Biol. Chem.* **278**, 7215–7219.

Collaborative Computational Project, Number 4 (1994). *Acta Cryst.* D**50**, 760–763.

Evans, S. V. (1993). *J. Mol. Graph.* **11**, 134–138.

Gurskaya, N. G., Fradkov, A. F., Terskikh, A., Matz, M. V., Labas, Y. A., Martynov, V. I., Yanushevich, Y. G., Lukyanov, K. A. & Lukyanov, S. A. (2001). *FEBS Lett.* **507**, 16–20.

Labas, Y. A., Gurskaya, N. G., Yanushevich, Y. G., Fradkov, A. F., Lukyanov, K. A., Lukyanov, S. A. & Matz, M. V. (2002). *Proc. Natl Acad. Sci. USA*, **99**, 4256–4261.

Laskowski, R. A., MacArthur, M. W., Moss, D. S. & Thornton, J. M. (1993). *J. Appl. Cryst.* **26**, 283–291.

McDonald, I. K. & Thornton, J. M. (1994). *J. Mol. Biol.* **238**, 777–793.

Martynov, V. I., Maksimov, B. I., Martynova, N. Y., Pakhomov, A. A., Gurskaya, N. G. & Lukyanov, S. A. (2003). *J. Biol. Chem.* **278**, 46288–46292.

Matz, M. V., Fradkov, A. F., Labas, Y. A., Savitsky, A. P., Zaraisky A. G., Markelov, M. L. & Lukyanov, S. A. (1999). *Nature Biotechnol.* **17**, 969–973.

Otwinowski, Z. & Minor, W. (1997). *Methods Enzymol.* **276**, 307–326.

Pakhomov, A. A., Martynova, N. Y., Gurskaya, N. G., Balashova, T. A. & Martynov, V. I. (2004). *Biochemistry (Mosc.)*, **69**, 901–908.

Remington, S. J., Wacher, R. M., Yarbrough, D. K., Branchaud, B., Anderson, D. C., Kallio, K. & Lukyanov, K. A. (2005). *Biochemistry*, **44**, 202–212.

Sack, J. S. (1988). *J. Mol. Graph.* **6**, 224–225.

Terskikh, A., Fradkov, A., Ermakova, G., Zaraisky, A., Tan, P., Kajava A. V., Zhao, X., Lukyanov, S., Matz, M., Kim, S., Weissman, I. & Siebert, P. (2000). *Science*, **290**, 1585–1588.

Thor, J. J. van, Gensch, T., Hellingwer, K. J. & Johnson, L. N. (2002). *Nature Struct. Biol.* **9**, 37–41.

Tsien, R. Y. (1998). *Annu. Rev. Biochem.* **67**, 509–544.

Verkhusha, V. V. & Lukyanov, K. K. (2004). *Nature Biotechnol.* **22**, 289–296.

Wallace, A. C., Laskowski, R. A. & Thornton, J. M. (1995). *Protein Eng.* **8**, 127–134.

Wiedenmann, J., Ivanchenko, S., Oswald, F., Schmitt, F., Rocker, C., Salih, A., Spindler, K. D. & Nienhaus, G. U. (2004). *Proc. Natl Acad. Sci. USA*, **101**, 15905–15910.

Wood, T. I., Barondeau, D. P., Hitomi, C., Kassmann, C. J., Tainer, J. A. & Getzoff, E. D. (2005). *Biochemistry*, **44**, 16211–16220.

Yanushevich, Y. G., Gurskaya, N. G., Staroverov, D. B., Lukyanov, S. A. & Lukyanov, K. A. (2003). *Bioorg. Khim.* **29**, 356–360.

Yarbrough, D., Wachter, R. M., Kallio, K., Matz, M. V. & Remington, S. J. (2001). *Proc. Natl Acad. Sci. USA*, **98**, 462–467.

Zubova, N. N., Bulavina, A. Y. & Savitski, A. P. (2003). *Uspekhi Biol. Khim.* **43**, 163–224.